Multiple Luminaire Identification in Airborne Images of Airport's Approach Lighting Using Mathematical Morphology With Variable Length Structuring Element

Shyama Prosad Chowdhury, Karen Rafferty and Stuart Ferguson
School of Electronics, Electrical Engineering and Computer Science
Queen's University Belfast, UK
schowdhury01@qub.ac.uk, {k.rafferty, r.ferguson}@ee.qub.ac.uk

***Abstract*—In night aviation, to land an aircraft, a pilot needs to be able to identify an airport. The approach lighting system (ALS) at an airport is used to provide identification and guidance to pilots. ALS consists of more than 100 luminaires which are installed in a defined pattern following strict guidelines by the International Civil Aviation Organization (ICAO). ICAO also has strict regulations for maintaining the performance level of the luminaires. However, to date there is no automated technique by which to monitor the performance of the lighting. We suggest using images of the lighting pattern captured using a camera placed inside an aircraft. Based on the information contained within these images, the performance of the luminaires has to be evaluated which requires identification of over 100 luminaires within the pattern of ALS image. This research proposes analysis of the pattern using morphology filters which use a variable length structuring element (VLSE). The dimension of the VLSE changes continuously within an image and varies for different images. A novel technique for automatic determination of the VLSE is proposed and it allows successful identification of the luminaires from the image data as verified through the use of simulated and real data.**

***Index Terms*—Approach lighting system, tracking of luminaires, pattern analysis, inter luminaire distance approximation, composite structure construction, block wise image analysis.**

I. Introduction

For this research, a camera is placed inside an aircraft and used to record a sequence of images of ALS luminaires when the aircraft is landing at an airport. This requires the identification and tracking of more than a hundred luminaires in over 150 images. In terms of shape features, luminaires are not individually identifiable as they have the same characteristics and do not have chromatic or texture distinction. Thus the various tracking technologies based on shape ([1], [2], [3], [4], [5], [6]), colour and texture features ([7], [8], [9], [10], [11]) that are used to solve different video processing tracking problems are not suitable for this particular application. For identification of the luminaires in each image we have exploited the positional information of the luminaires by using pattern based identification. This is a top-down procedure where a pattern is divided into a number of building blocks. Using these building blocks the overall pattern can be estimated.

(a) (b)

Fig. 1. (a) Original image of ALS (b) Localised luminaires in the image

In order to identify luminaires using the pattern based technique, it is first necessary to localise all luminaire data in the images. This localisation is achieved using the Iso-Illuminated Ridge (IIR) image analysing technique as described by Chowdhury et al. [12]. An example of the airborne ALS image is shown in Fig. 1(a) and the result of IIR analysis based localised luminaires is shown in Fig. 1(b). However, as the luminaires are closely placed with each other in an image, it is quite often that they are not individually segmented [55] after the IIR analysis. Vibration in the sensor plane when recording an image may turn the situation worse as luminaires form streak in the image due to heavy movement in the sensor plane [49]. Streaks of the multiple luminaires overlap with each other and form a single localised connected component. Thus, the individual connected component for each luminaire is not obtained for most of the luminaires unless the camera is close to that luminaire and that image is recorded without vibration. The localisation process often map several luminaires to a single component. Thus it is not possible to map directly the localised luminaire to the ALS pattern. It needs several steps to identify each luminaire inside the localised components, which may represent several luminaires clubbed together. From the localised luminaire data, a basic concept for prediction of the VLSE to be used in an

image is given in [13]. The current research paper extends that concept in several ways. The novel research contributions of this paper can be described as;

1) Formulation of a number of nonlinear mathematical models of inter luminaire distance for the ALS pattern in an airborne image are proposed in section III-A1. Modelling is done for any two luminaires which are either separated horizontally or vertically. These models are also experimentally verified, see Fig. 6 and Fig. 7.
2) A new technique for the fully automatic analysis of an airborne ALS image is presented to retrieve values of the different parameters which are used in these parametric models (section III-A2). These retrieved values for the parameters along with the proposed model are then used to construct a number of VLSEs which are used for several mathematical morphology operations. Detailed description of these morphological operations are presented in sections III-A3, III-A4 and III-B.
3) The proposed modelling technique for two vertically separated luminaires is further extended to analyse blocks inside the overall ALS pattern. This technique is developed using a nonlinear analysis on the image coordinate system with respect to the known ALS pattern. This proposed technique is detailed in section III-B1.

Following this introduction, a review of related research is presented in section II, this will help place in context the novelty we have described. A pattern based identification method is proposed and described in section III. The experimental results for the pattern based identification is presented in section IV. Finally a summary of the localisation and tracking technique is detailed in section V.

II. Related Research

Use of morphological filters for analysis of images is a popular area of research in image processing [14]. Goutsias et al. [15] described the morphological representation of the discrete and binary image. Statistical analysis of the morphological opening is described in [16] whereas evolution of the filtering is explained by Brockett et al. in [17]. Spatially variant morphology restoration and skeleton representation is studied by Bouaynaya et al. in [18]. A detailed description of the spatially variant mathematical morphology for binary and grey images can be found in [19] and [20]. Spatially variant structuring elements (SVSE) were first described by Serra [21] in the binary case. Heijmans [22] includes spatially variant definition for all morphological operators and not limited to the binary case. Image filtering using morphological amoebas explained by Lerallut et al. [23]. Dokladal [24] used fast methods for their implementation and proposed an extension to 2-D with resizable rectangles. Tankyevych et al. [25] presented a combined linear-morphological filter for detecting, edge-enhancing and reconnecting blood vessels on real 3D CTA data. A generic morphological algorithm is described by Levillain et al. in [26]. A unification of morphological and fuzzy algebraic systems for lattice image processing is explain by Maragos in [27]. Microarray gridding by mathematical morphology is explained by Hirata et al. in [28] and segmentation of these images are detailed in [29].

An overview of adaptive morphology, its trend and perspective is described by Maragos et al. in [30]. Ito et al. [31] define a new adaptive morphological operation, in which the value of a structuring element varies adaptively depending on the local intensity information of the processing image of interest. Traffic spatial measurement using video image processing is reported by Beucher et al. [32]. Cuisenaire [33] investigated how common binary mathematical morphology operators can be adapted so that the size of the structuring element can vary across the image pixels. Dias et al. [34] applies the morphological filter in simplicial complex spaces whereas the morphological operators are used in graph space in [35]. It is applied for the motion segmentation by Hirata et al. in [36] as well as for the text segmentation [37]. Mapping of sub-watersheds from a digital elevation model is experimented by Chockalingam et al. in [38]. Das et al. [39] used morphology to correct skew in a document page. Najman et al. [40] reviews skew detection technique in document image. A basic paradigm in mathematical morphology is the construction of a set operators by concatenations of dilations and erosions via the operations of composition, union, intersection and complement; Barrera et al. [41] describe designing a Hybrid human machine binary morphological operator. A partial differential equations (PDE) formulation for viscous morphological operators with extensions to intensity-adaptive operators is detailed by Maragos et al. in [42]. Lim et al. [43] uses Morphological convexity measures for terrestrial basins derived from digital elevation models.

Whilst the application of morphological operators are applied in almost every domain of image processing where spatial information is of prime concern, it is not used for identification and tracking of the luminaires in airport lighting. Niblock et al. [44] studied the application of two existing tracking techniques applied to airport lighting image data. These being the Kanade−Lucus−Tomasi (KLT) [45], [46] and scale invariant feature transform (SIFT) [47], [48]. In their study, Niblock et al. concluded that both of these techniques show very poor success rate. The KLT performed at $\sim 60\%$ accuracy whereas SIFT has shown only $\sim 20\%$ success rate [44].

To overcome the poor accuracy of tracking the luminaires, Niblock et al. proposed a fast model based feature matching technique [44]. Initially they constructed a template based on the ALS luminaire data. Then using an optimising technique, the template is superimposed on the acquired image data. The objective of this optimisation is to achieve a one-to-one match between the template and the luminaire data. Using this technique they achieved a $\sim 76\%$ success rate which is higher than that of the KLT and SIFT technique. This model based technique [44] is a good example of bottom-up approach. All the luminaires need to be mapped individually with the corresponding entity in the model or template to define the final pattern of the ALS. However, in their approach Niblock et al. did not make any provision for matching different subsets of luminaires to match the template individually. In addition, the success ratio was determined using very limited data, that is two approach sequences to an airport which were acquired under similar operating conditions.

The main objective of developing the presented pattern based identification technique was to enhance the accuracy and robustness of the tracking technique proposed by Niblock, and to more robustly and scientifically test the new approach. Thus a new algorithm must be capable of identifying the position of all luminaires within an image and tracking them between images. This information is used to label all the extracted luminaires from the image for performance assessment [49].

III. Pattern Based Identification

Images of the ALS were taken using a camera which is mounted in the cockpit of an aircraft. Along with the aircraft, the camera has also 6 degrees of freedom. Thus, images of the ALS are frequently rotated in the 2D image plane of the camera. Thus the images are preprocessed to remove skew from the ALS pattern which simplifies the tracking. This is described in section III-A. Section III-B outlines the technique that has been implemented for identification.

A. Skew Correction of ALS Pattern in Image

The ALS is physically made up of 120 luminaires which are distributed along a centreline and five crossbars. In an ideal situation, the centreline and crossbars should appear in the vertical and horizontal directions of the image plane. Typically however they appear skewed within the image. It is necessary to remove the skew to simplify luminaire tracking. In order to remove the skew from the crossbars a two step technique is used. The first step being major skew correction (MSC) which is detailed in [12] and the second step being finer skew correction (FSC) using VLSE in the morphology filter.

MSC requires identification of the control points which are used for a tentative prediction and correction of any higher amount of skew with lesser accuracy. The top luminaire in the centreline is chosen as control point (CP). From CP two horizontal straight lines are formed on both the left and right side of the pattern. The left line is rotated anticlockwise and the right line clockwise until they intersect with luminaires outer boundary which we call the Iso-Illuminated Ridge Line (IIRL). Here, IIRL is obtained in a two steps procedure that includes Iso-illuminated Ridge (IIR) image construction and IIRL marking ([12]). In IIR construction phase bit information of an pixel is considered. For a single byte camera, each byte of information is made up from 8 single bits, each of which hold information regarding that pixel. In a byte, 8 bits (0 to 7) have their different positional weightage factor. Typically the bit at location 7, is termed the most significant bit (MSB). And the bit at location 0, is termed the least significant bit (LSB).By omitting the MSB the highest value of that byte will decreased to 127. To keep the highest value in the same range, the value is multiplied by a factor 2. Similarly after omitting the two MSBs, the value is multiplied by a factor 2^2. After the omission of the MSB and the two MSBs changes in the bell shaped curve a significant edge profile for the luminaire, making it easier to detect. When the ridges are constructed, a discontinuity in the ridge can be associated with the edge of a luminaire. These ridges are marked as IIRL.

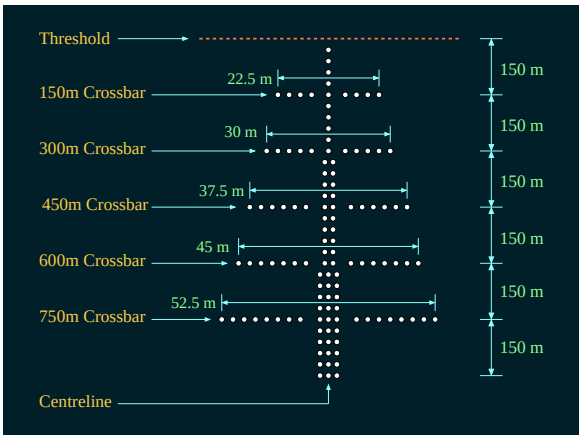

Fig. 2. Physical placement of the luminaires in ALS pattern

For two projected straight lines from CP, let the final touch points on the same crossbar by the left and the right lines be the $P^{(l)}$ and $P^{(r)}$ consecutively. Thus, any touch point is the topmost point of a luminaire in an IIRL image. A vertical traverse from any of the touch point to the bottommost position of that component will be a traverse through the vertical cross section of that luminaire. Let the traversed middle points of the two luminaires having the touch points $P^{(l)}$ and $P^{(r)}$ be $P^{(l)}_{mid}$ and $P^{(r)}_{mid}$ consecutively. These middle points are the centre points of the leftmost and rightmost luminaires of a crossbar. Thus the skew of the straight line formed by these two points is the tentative skew of the luminaire model. The angle function $Ang(x, y)$ finds the angle in between two points x and y. Thus the angle between the points $P^{(l)}_m$ and $P^{(r)}_m$ is $\beta_M = Ang\left(P^{(l)}_m,\ P^{(r)}_m\right)$. The image is then rotated $-\beta_M$ to correct the major skew and obtain $(I^{(M)})$.

FSC is achieved by measuring the deflection of the crossbars from the horizontal direction. In order to determine the crossbars, morphological filters are utilised. Use of a fixed structuring element (SE) [50] for analysing the positional information of luminaires in the image is not suitable because luminaires appear much smaller at the far end of an image compared to those which are nearer to the camera. Such perspective distortion also effects the inter luminaire distance in the image, which is higher when luminaires are near to the camera. Thus to find a suitable SE which will work irrespective of having variable sizes of luminaires and inter luminaire distances throughout the image, we have proposed morphological operations that are undertaken using a VLSE, the length of which is determined intelligently from the image data. The process of creating VLSE is now described.

1) Modelling Distance between Two Luminaires: In the physical model on the ALS the distance between two centreline luminaires or the distance between two crossbar luminaires (Fig. 2) is the same (as necessitated by the ICAO standards [51]). However because images captured using a camera suffer from perspective projection the corresponding pixel distance between two adjacent luminaires varies according to the location of the luminaires within the captured image. As the row index increases downwards, the distance between

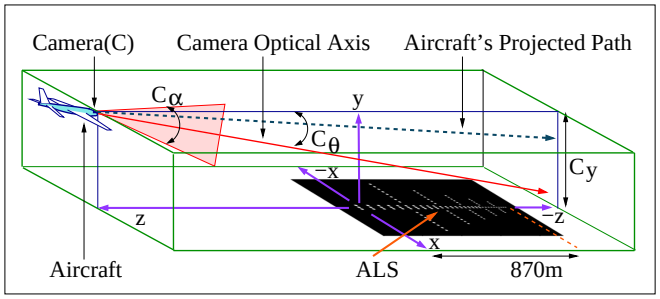

Fig. 3. Side view: An aircraft approaching towards the runway

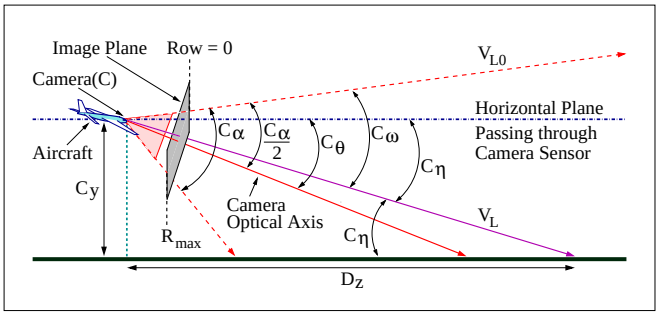

Fig. 4. Angular relation between physical placement of objects, image plane and camera FOV in a vertical cross section

luminaires in the image also increases. This variability necessitates the use of a VLSE which is determined as follows.

The vertical field of view (FOV) angle of the camera is C_α (Fig. 3 and Fig. 4) and the pitch angle is C_θ. The row value at the top most position of the image is 0 and at the bottom it is R_{max}. Within the FOV of the camera, the view-line (V_L) is a straight line that connects any physical location to the camera. For example, a V_L can connect the camera to the object which appears at row 0 in the image (V_{L0}). Any other V_L creates a vertical angle (C_ω) with V_{L0}. This angle is also a linear function of the row position (R) in an image. If the row index increases then C_ω also increases linearly. Similarly, value of C_ω is 0 at the top most position whereas it is C_α at the bottom. Thus,

$$C_\omega \;=\; \left(\frac{C_\alpha}{R_{max}}\right) R\,. \tag{1}$$

Any V_L creates a vertical angle C_η with the horizontal plane associated with the camera coordinate system. This C_η is a composite angle which is a function of pitch angle (C_θ) of the camera, vertical FOV angle (C_α) and vertical angle of the V_L with V_{L0} (C_ω) (Fig. 4). Expanding this composite angle it can be obtained as

$$C_\eta \;=\; C_\theta \;-\; \frac{C_\alpha}{2} \;+\; C_\omega\,. \tag{2}$$

Thus, using (1) and (2)

$$C_\eta \;=\; C_\theta \;-\; \frac{C_\alpha}{2} \;+\; \frac{C_\alpha R}{R_{max}}\,. \tag{3}$$

At any instant, the height of the camera above the ground is C_y. Let the horizontal distance between the camera and the physical point touched by V_L be D_z. Then the ratio $\frac{D_z}{C_y}$ is the cotangent function of the angle C_η,

$$\frac{D_z}{C_y} \;=\; cot\left(C_\theta \;-\; \frac{C_\alpha}{2} \;+\; \frac{C_\alpha R}{R_{max}}\right). \tag{4}$$

As described earlier because of perspective projection, the pixel distance between two equi-distant objects can vary, dependent on where these objects are in the image plane. To find the variation along the rows, the derivative of D_z is calculated with respect to row (R) as follows:

$$\frac{dD_z}{dR} \;=\; cosec^2\left(C_\theta \;-\; \frac{C_\alpha}{2} \;+\; \frac{C_\alpha R}{R_{max}}\right)\left[\frac{-C_y C_\alpha}{R_{max}}\right]. \tag{5}$$

Thus the variation of the distance D_z per pixel in row (R) is

$$dD_z^{(u)} \;=\; cosec^2\left(C_\theta \;-\; \frac{C_\alpha}{2} \;+\; \frac{C_\alpha R}{R_{max}}\right)\left[\frac{-C_y C_\alpha}{R_{max}}\right]. \tag{6}$$

If two object points that are physically separated by a unit distance $D_x\ (=1)$ and in the image they register in same row position then the pixel distance between these object points D_H will be

$$\begin{aligned} D_H \;&=\; \frac{D_x}{dD_z^{(u)}} \\ &=\; sin^2\left(C_\theta \;-\; \frac{C_\alpha}{2} \;+\; \frac{C_\alpha R}{R_{max}}\right)\left[\frac{-R_{max}}{C_y C_\alpha}\right]. \end{aligned} \tag{7}$$

Using (3) and (7), D_H can be written as

$$D_H \;=\; \frac{D_x}{dD_z^{(u)}} \;=\; sin^2(C_\eta)\left[\frac{-R_{max}}{C_y C_\alpha}\right]. \tag{8}$$

Practically the angle C_η in radians will be less than 1. Expanding the term $sin^2(C_\eta)$ then

$$sin^2(C_\eta) \;=\; C_\eta^2 \;-\; \frac{C_\eta^4}{3} \;+\; \frac{2C_\eta^6}{45} \;-\; \ldots\,. \tag{9}$$

Here the higher order terms of C_η can be practically ignored as C_η is much less than 1. The value of D_H from (7), (9) and (3) can be written as,

$$D_H \;=\; \left(C_\theta \;-\; \frac{C_\alpha}{2} \;+\; \frac{C_\alpha R}{R_{max}}\right)^2\left[\frac{-R_{max}}{C_y C_\alpha}\right]. \tag{10}$$

This can be simplified to,

$$\begin{aligned} D_H \;&=\; -\left(\frac{C_\alpha}{C_y R_{max}}\right)R^2 \;+\; \left(\frac{C_\alpha - 2C_\theta}{C_y}\right)R \\ &\quad -\; \frac{(C_\alpha - 2C_\theta)^2 R_{max}}{4C_y C_\alpha}. \end{aligned} \tag{11}$$

Thus, D_H can be represented as a second order polynomial function of R. It implies that for all equidistant luminaires, the displacement in the image will be a quadratic function of the row value (R). From Fig. 4 and Fig. 1(a) it can also be verified that $\frac{C_\alpha}{2} > C_\theta$ which means $(C_\alpha - 2C_\theta) > 0$. Thus, (11) can be written as

$$D_H \;=\; -K_1 R^2 \;+\; K_2 R \;-\; K_3 \tag{12}$$

where, K_1, K_2 and K_3 are the positive constants. Having a negative coefficient $(-K_1)$ associated with R^2 signifies that

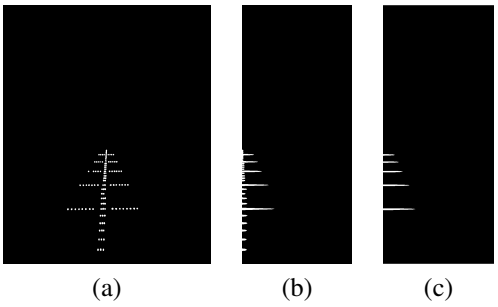

(a) (b) (c)

Fig. 5. (a) Major skew corrected image (b) Horizontal projection of detected luminaire (c) Crossbar bands from the horizontal projection

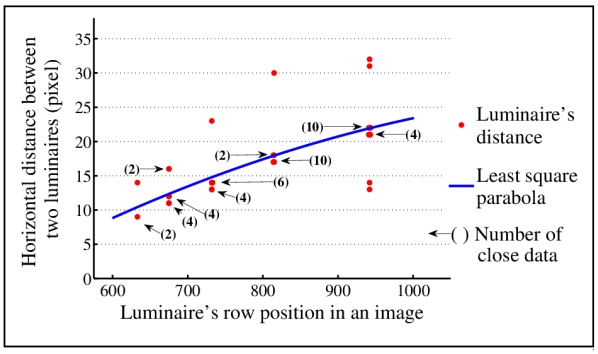

Fig. 6. Horizontal distance of two luminaires in an image

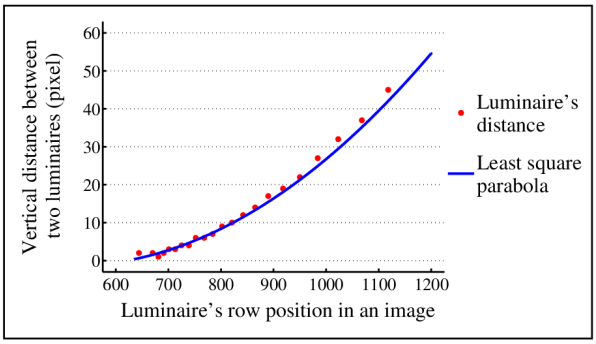

Fig. 7. Vertical distance of two luminaires in an image

this quadratic equation will generate a parabola that opens downwards.

The distance between two objects that are separated by an unit distance (D_H) itself changes in the different row position (12). Thus, (D_H) can only be used to measure distance between two objects which appear horizontally or almost horizontally in the image. Using (12), changes in the pixel distance for changes in rows between two objects that are separated by a unit distance can be written as

$$\frac{dD_H}{dR} \;=\; -2K_1R \;+\; K_2. \tag{13}$$

Also in the image plane, the measure of unit distance changes along the rows following $\frac{dD_H}{dR}$. Thus for two objects that are separated vertically, the distance can be formulated as

$$D_V \;=\; \left(\frac{dD_H}{dR}\right)^2 \;=\; 4K_1^2R^2 \;-\; 4K_1K_2R \;+\; K_2^2. \tag{14}$$

Thus, D_V is a quadratic function of row R. Here, R^2 is associated with a positive constant which signifies this quadratic equation will generate a parabola that opens upwards. Using (12) and (14) it is possible to estimate the pixel difference between luminaires in the horizontal and vertical directions in an image. This is now explained in details.

2) Finding Inter Luminaire Distance at Different Image Location: For measuring D_H at different rows, crossbar luminaires are considered and all other luminaires are intentionally ignored. Initially a horizontal projection is taken of all the detected luminaire pixels to find the rows that contains the crossbar luminaires. An example image and its horizontal projection is shown in Fig. 5(a) and (b). From this projection profile, bands for crossbars are detected (Fig. 5(c)) using a mealy machine [52] whose output is associated with state transitions which are controlled by a set of basic statistical measures.

The intermediate horizontal distance between two consecutive crossbar luminaires is measured and a second order polynomial is fitted on these measured distances. It is shown that if the distance between consecutive equi-distant luminaires is plotted as a function of row position, then a least square parabola (LSP) is the best fit for that data (Fig. 6). Thus this LSP which is named as L_H represents D_H and will allow us to automatically determine the width of the best VLSE to perform the morphological operations. Fig. 6 illustrates the inter luminaire distance between crossbar luminaires which are almost the same (except the distances calculated with centreline luminaires) for a given crossbar. The LSP obtained from these plots, also opens downwards. This is further proven by the relationship derived in (12).

For establishing a parametric relation between the row position and distance between vertically separated consecutive luminaires, the inter luminaire distance is measured column wise. Following (14), the vertical displacement is a quadratic function of row value. Thus, a second order polynomial is fitted on these measured distances (Fig. 7). This best fit LSP (L_V) on the vertically measured distance will be used for determining height of the best VLSE to perform morphological operations and tracking the luminaires.

3) Composite Structure Construction: A composite structure is created because it is an initial requirement for the pattern analysis. Let V_C be the structuring element used for binary morphological closing on a binary input image where, the height and width of this VLSE are denoted by $V_C^{(H)}$ and $V_C^{(W)}$. Both $V_C^{(H)}$ and $V_C^{(W)}$ are two dimensional image functions where, $V_C^{(H)}(i,j)$ and $V_C^{(W)}(i,j)$ represents the height and width of the VLSE on a pixel in i^{th} row and j^{th} column. Here $V_C^{(H)}(i,j) = \lambda_1 L_V(i)$ and $V_C^{(W)}(i,j) = \lambda_2 L_H(i)$ where, $L_V(i)$ and $L_H(i)$ are the value of the least squares parabola at the i^{th} row. Note that both the $L_V(i)$ and $L_H(i)$ are monotonically increasing functions. Thus, the dimension of the VLSE increases with the increasing value of row number. The value of λ_1 is kept constant at 2 and λ_2 at 6. Morphological closing [21][53] on an $I^{(M)}$ image which is a binary image with structuring element V_C results in a single

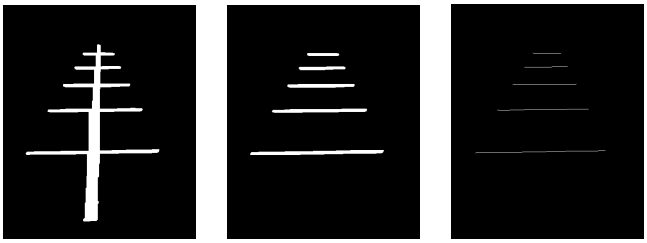

(a) (b) (c)

Fig. 8. (a) Composite structure after closing (b) Detected crossbars after opening (c) Skeleton of the crossbars after thinning

structure (Fig. 8(a)) with all the luminaires [13]. This image will later be referred to as as $I^{(C)}$.

$$I^{(C)} \quad = \quad I^{(M)} \bullet V_C. \tag{15}$$

4) Crossbars Extraction: Let V_O denote the structuring element used for binary morphological opening, where the height and width of this VLSE are denoted by $V_O^{(H)}$ and $V_O^{(W)}$. Opening is performed on $I^{(C)}$ which is also a binary image with a horizontal line like structuring element. Thus, $V_O^{(H)}$ is of a constant value 1 and $V_O^{(W)}(i,j) = \lambda_3 L_R(i)$. The value of λ_3 is held constant at 3 to ensure that the opening element will definitely remove the centreline links between crossbars to form an output as shown in Fig. 8(b). This image will be known as $I^{(O)}$ for the next stages [13].

$$I^{(O)} \quad = \quad I^{(C)} \circ V_O. \tag{16}$$

5) Deflection Angle Calculation: A thinning algorithm [54] is applied to the remaining objects after binary morphology opening (Fig. 8(c)). An 8-connected component analysis (8-CCA) on the skeleton of the crossbars will label all the skeleton lines. Let us assume a total T $(1 \leq T \leq 5)$ number of components are present where the spread of the k^{th} component is from the point $P_k^{(l)}$ to $P_k^{(r)}$. The distance function $Dist(x,y)$ determines the distance in between two points x and y. As defined earlier, the angle function $Ang(x,y)$ measures the angle. A weighted average deflection of all the crossbars from the horizontal line is calculated as β_F where,

$$\beta_F = \frac{\sum_{k=1}^{T} \left(Dist\left(P_k^{(l)},\ P_k^{(r)}\right)\ Ang\left(P_k^{(l)},\ P_k^{(r)}\right)\right)}{\sum_{k=1}^{T} Dist\left(P_k^{(l)},\ P_k^{(r)}\right)}. \tag{17}$$

The major skew corrected image $(I^{(M)})$, morphologically closed composite structure image $(I^{(C)})$ and morphologically opened image $(I^{(O)})$ are then rotated with the $-\beta_F$ angle to get the $I_R^{(M)}$, $I_R^{(C)}$ and $I_R^{(O)}$ which are fully skew corrected and all the crossbars become horizontally aligned [13]. The error associated with formation of the thinned lines are less than 1 pixel. The average length of the longest thin line is always more than 114 pixels thus the skew is corrected up to 0.5° as $\tan^{-1}\frac{1}{114} = 0.5^\circ$.

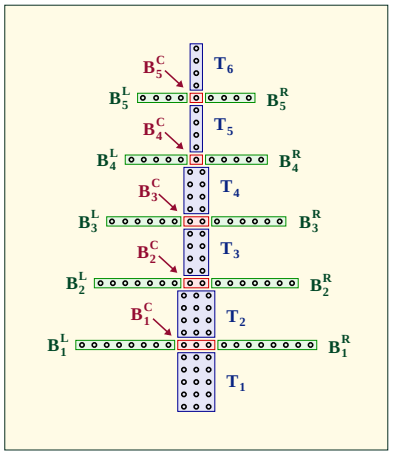

Fig. 9. Control blocks in ALS

B. Pattern Based Identification of ALS Luminaires

The ALS pattern is further analysed so that it can be mapped onto a number of control blocks. The crossbars are labelled $(B_k, 1 \leq k \leq 5)$. For all the 120 luminaires in the ALS, 21 basic blocks are formed as shown in Fig. 9. Crossbars have two wings spread on both sides of the centre body which is aligned with the centreline. The two wings and the centre body of the k^{th} crossbar are named as $B^L{}_k$, $B^R{}_k$ and $B^C{}_k$ where, $1 \leq k \leq 5$. Part of the centreline on top of the 5^{th} crossbar (B_5) is labelled as T_6 and all other parts of the centreline in between k^{th} and $(k+1)^{\text{th}}$ crossbars $((B_k, (B_{k+1})$ are labelled as T_{k+1} $(1 \leq k \leq 4)$. Part of the centreline below the first crossbar is labelled as T_1. A total 6 centreline blocks can be labelled here.

Having created a method to label the luminaires, they now must be identified between images. At this stage we have generated a composite pattern image $I_R^{(C)}$ and the detected centreline image $I_R^{(O)}$. These two images are binary morphologically dilated with a VLSE denoted by V_D to envelop on the luminaires in image $I_R^{(M)}$. The height and width of this VLSE are denoted by $V_D^{(H)}$ and $V_D^{(W)}$ which is a fraction of the inter luminaire distances as $V_D^{(H)}(i,j) = \lambda_4 L_V(i)$ and $V_D^{(W)}(i,j) = \lambda_5 L_H(i)$ where, $\lambda_4 = 0.2$ and $\lambda_5 = 0.4$. An example of an enveloped luminaire in $I_R^{(C)}$ by the dilated composite structure is $I_D^{(C)}$ and shown in Fig. 10(a). Dilation on $I_R^{(O)}$ forms $I_D^{(O)}$ (Fig. 10(b)) that envelops all the crossbars that are present in $I_R^{(M)}$.

$$I_D^{(O)} \quad = \quad I_R^{(O)} \oplus V_D. \tag{18}$$

1) Identifying Centreline Blocks: The enveloped crossbar ($I_D^{(O)}$, Fig. 10(b)) is subtracted from the enveloped composite structure ($I_D^{(C)}$, Fig. 10(a)) to obtain the centreline blocks N in the image. That is,

$$N \quad = \quad I_D^{(C)} \ - \ I_D^{(O)}. \tag{19}$$

In each of the centreline blocks, binary morphological closing is carried out with a VLSE (V_O). This generates a vertical sequence of regions which are enveloped in a rectangular strip and shown in Fig. 10(c). For a given block if the expected

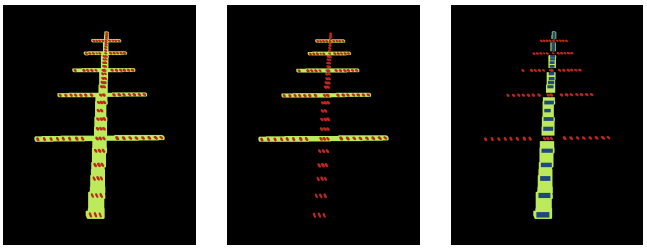

(a) (b)

Fig. 10. (a) Enveloped composite structure (b) Enveloped crossbars (c) Regions inside the centreline blocks

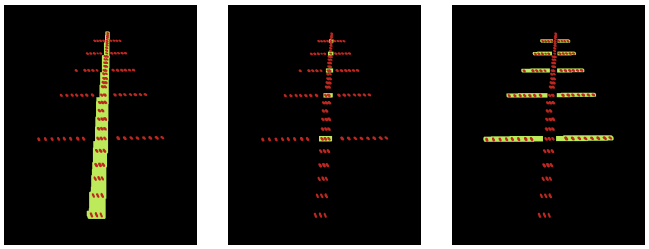

(a) (b) (c)

Fig. 11. (a) Detected complete centreline (b) Centre body blocks (c) Wing blocks

number of strips are not found then the centreline block is divided into that expected number of pieces. Initially it is divided into two halves and then each half is divided again into another two halves. However, the division of the regions into two halves cannot be linear because of the perspective error. Let us consider that we have to divide a centreline block which is of height D rows and spans from row R_t to R_b. Travelling downwards from R_t, let us arrive at the row position R_m that intersects the block into two equal halves (in the physical ALS plane) of row height D_1 and D_2. That means

$$D_1 = R_m - R_t , \quad (20)$$

$$D_2 = R_b - R_m \quad \text{and} \quad (21)$$

$$D = D_1 + D_2 = R_b - R_t. \quad (22)$$

Taking R_m as the mid point of row value R_t and R_b yields the wrong result as the row distance is not linear but on a parabolic curve. Thus to calculate the actual difference, non linear approximation, L_V, is used.

Considering D_1 as the p times the vertical inter luminaire distance measured from row R_t. Then following (14),

$$D_1 = pK'_1R_t^2 + pK'_2R_t + pK'_3. \quad (23)$$

where, $K'_1 = 4K_1^2$, $K'_2 = -4K_1K_2$ and $K'_3 = K_2^2$ are obtained from least square approximation (as described in (14) and explained with Fig. 7). As both D_1 and D_2 represent same distance and D_1 is p times the vertical inter luminaire distance measured from row R_t, then D_2 has to be p times the vertical inter luminaire distance when measured from row R_m. This is written as

$$D_2 = pK'_1R_m^2 + pK'_2R_m + pK'_3. \quad (24)$$

Using (20), the the unknown term R_m in relation (24) can be excluded as

$$D_2 = pK'_1(D_1 + R_t)^2 + pK'_2(D_1 + R_t) + pK'_3. \quad (25)$$

Thus using (23) and (25)

$$D_2 = pK'_1D_1^2 + (2pK'_1R_t + pK'_2 + 1)D_1. \quad (26)$$

Here, using (22), (23) and (26) a quadratic equation for D_1 can be written as

$$pK'_1D_1^2 + (2pK'_1R_t + pK'_2 + 2)D_1 - D = 0. \quad (27)$$

Solving this by taking the positive square root of the discriminant, the value of D_1 in the linear scale can be computed. Thus using (20) and (27) the desired R_m that will divide the block into two equal halves when p is given can be determined. If all the expected components are available inside a strip then those are identified otherwise using the previously calculated inter luminaire approximation L_H is applied for prediction of the horizontally separated luminaires.

2) Identifying Centre Body Blocks: On the detected envelop of the centerline blocks (N), binary morphological closing is carried out with a VLSE denoted by V_{C1} and similar to the vertical line. The width of this VLSE is 1 and height is denoted by $V_{C1}^{(H)}$ and calculated as $V_{C1}^{(H)}(i,j) = \lambda_6 L_V(i)$. The complete centreline which is obtained after the closing operation (E) the result of which is shown in Fig. 11(a).

$$E = N \bullet V_{C1}. \quad (28)$$

An intersection of the enveloped crossbar ($I_D^{(O)}$, Fig. 10(b)) and the complete enveloped centreline (E, Fig. 11(a)) generates an enveloped image of the centre body luminaires as shown in Fig. 11(b). Let this image be known as Y^C. Then,

$$Y^C = E \cap I_D^{(O)}. \quad (29)$$

For the k^{th} centre body block the maximum number of horizontally separated luminaires is $\lfloor \frac{7-k}{2} \rfloor$ where, $\lfloor a \rfloor$ represents the previous higher integer or floor value of a. For each centre body block, a 8-CCA is then applied. If all the expected components are available inside a centre body block then those are identified, otherwise using the previously calculated inter luminaire approximation, L_H is applied for prediction of the horizontally separated luminaires.

3) Identifying Wing Blocks: To detect the wing bars, the complete centreline (E, Fig. 11(a)) is subtracted from the enveloped composite structure ($I_D^{(C)}$, Fig. 10(a)). This can be written as

$$Y^W = I_D^{(C)} - E. \quad (30)$$

where, Y^W contains all the wing blocks with an envelop. An example image is shown in Fig. 11(c). All the left sided wing blocks are numbered from $Y^L{}_5$ to $Y^C{}_1$ whereas all the right sided blocks are numbered from $Y^R{}_5$ to $Y^R{}_1$. If the expected number and the detected number of luminaires does not match then by using a least square approximation of the separated luminaires L_H, position and width of the detected component can be analysed.

TABLE I
SUCCESS RATE OF THE TRACKING TECHNIQUES

Parameters under measurement		Success Rate (%)
Experiment number	Vibration (%)	Pattern based identification
Ori-1	-	92
Ori-2	-	94
Sim-1	1.13	92
Sim-2	1.76	92
Sim-3	0.85	94
Sim-4	1.09	93
Sim-5	1.22	92
Sim-6	2.14	90
Sim-7	1.61	91
Sim-8	1.75	93

IV. RESULTS

The pattern based identification technique for tracking the ALS luminaires introduced in this paper has been tested with a large number of data sets. This includes two sets of real videos taken during an approach to an airport in Northern Ireland and eight sets of simulated image sequences as generated using the technique described in [55]. Each video has approximately 200 images. Thus $\sim$ 400 real images and $\sim$ 1600 simulated images were tested using the proposed technique. As the ALS is comprised of 120 luminaires, around 200 images demand identification and tracking of more than $15,000$ instances of luminaires. Thus, for 10 sets of data, $150,000$ instances of luminaires must be identified and tracked. In this experiment it has been assumed that testing on this quantity of data should generate an overall view as to how the proposed algorithms perform. The success rate of the tracking is measured in each image as

$$\text{Success rate}(\%) = \frac{N_{predict} \times 100}{N_{total}} \tag{31}$$

Here, $N_{predict}$ is the number of successfully predicted luminaires and N_{total} is the number of total luminaires present in that image.

Table I outlines the percentage of the number of successfully identified and tracked luminaires per image. The result of the detected luminaires of the are shown in Fig. 12(a) to (j). Using the proposed pattern based identification, the tracking accuracy is around 90% to 94%. However, this cannot track the luminaires which are near the bottom boundary of the image and about to leave the image. This is due to the fact that the morphological operation does not get enough room to adequately perform. The pattern based identification technique produces a good success rate otherwise. It is also interesting to note that the processing time for processing a 1280×1024 image using the pattern based identification of luminaires takes around 0.8 second per image whereas for an image of size 800×640, pattern based identification takes around 0.6 second per image. Here all the codes are developed in C language using the standard libraries.

It has already been reported in [44] that the existing KLT and SIFT techniques give $< 60\%$ and $< 20\%$ success rates in tracking luminaires, whereas model based matching techniques produce a 76% success rate. An experiment to compare the proposed pattern based identification technique with the model based matching technique was performed using the real image data. Fig. 13(a) shows the number of correctly predicted luminaires for an image sequence using both of these tracking techniques. In Fig. 13(a), the result is presented on a subset of real images taken at Belfast International Airport. In the full data set there are 207 images. Among these, 20 images were not properly recorded and the existing performance evaluation algorithm [49] cannot run on luminaire data from those 20. On the remaining 187 images we have carried out the luminaire's performance evaluation process and we call these images, candidate images. The target is to correctly identify the luminaires in all the 187 candidate images. Using the proposed pattern based identification technique, we have obtained identification

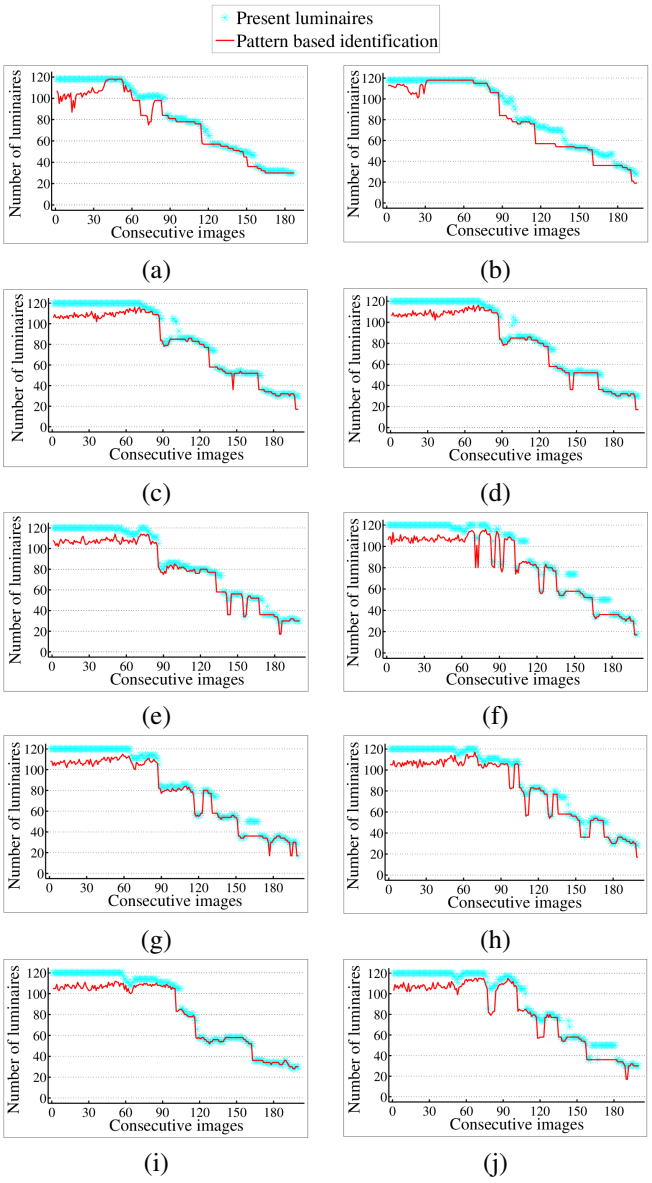

Fig. 12. Number of luminaires present in an image and correct prediction of luminaires' position by Pattern based identification in (a) Ori-1 (b) Ori-2 (c) Sim-1 (d) Sim-2 (e) Sim-3 (f) Sim-4 (g) Sim-5 (h) Sim-6 (i) Sim-7 (j) Sim-8 image sequences

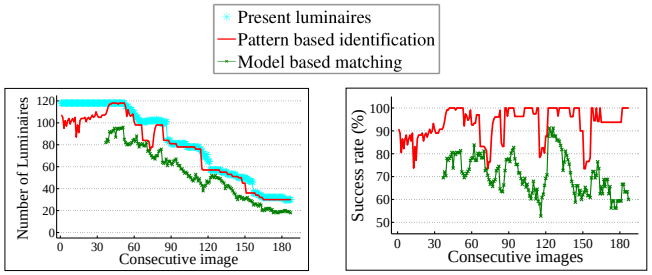

(a) (b)

Fig. 13. Using pattern based identification and model based matching techniques (a) Number of luminaires present in an image and correct prediction of luminaires' position (b) Success rate (%) of correctly predict the luminaires

result in each of the 187 images. However, using model based matching technique, a successful result is obtained in only 151 images. Because of the distance between the camera and luminaires, the first few images show the ALS pattern within a small area on image. The model based matching technique does not produce a successful outcome in the first 36 images. The success rate of predicting the luminaires per image is shown in Fig. 13(b).

When calculating result on the last 151 candidate images, it is found that the model based matching technique gives an overall success rate of 72%. The pattern based identification can predict with a 94% success rate. If all the 187 candidate images are considered then the proposed pattern based identification technique shows a 92% success rate whilst the model based matching technique demonstrates only 52%. Thus the proposed identification techniques outperforms other published tracking algorithms in the area [44]. This would suggestion that the application of variable length structuring elements is incredibly useful in certain tracking applications.

V. Conclusion

In the presented pattern based identification technique a fully automatic procedure is proposed which exploits knowledge of the luminaire pattern. A novel construction of the VLSE is achieved which will change dependent on the location in an image. Constructing the SE for morphological operation is always a challenging task and we have achieved this intelligently by exploiting knowledge of the pattern and approximating the inter luminaire distance in the image. Development of this pattern based identification method helps achieve an autonomous technique for tracking the luminaires in the ALS pattern. It can identify the luminaire correctly and can also predict the position of luminaires which are not detected. This technique has the major advantage of not requiring any external parameters such as camera position with respect to the pattern, sensor characteristics, distortion model for the lens etc. Every parameter in this proposed technique is self generated from either the pattern or the image itself. The result is encouraging and it shows that the proposed identification technique outperforms other available methods to date. This work has utility in many application areas, for example, where multiple similar objects need to be tracked over a period of time.

References

[1] D. Cremers, "Dynamical statistical shape priors for level set-based tracking," *IEEE Transactions on Pattern Analysis and Machine Intelligence (PAMI)*, vol. 28, no. 8, pp. 1262 – 1273, 2006.

[2] T. Kim, S. Lee, and J. Paik, "Combined shape and feature-based video analysis and its application to non-rigid object tracking," *IET Image Processing*, vol. 5, no. 1, pp. 87 – 100, February 2011.

[3] S.-W. Lee, J. Kang, J. Shin, and J. Paik, "Hierarchical active shape model with motion prediction for real-time tracking of non-rigid objects," *IET Computer Vision*, vol. 1, no. 1, pp. 17 – 24, 2007.

[4] Y. Rathi, N. Vaswani, and A. Tannenbaum, "A generic framework for tracking using particle filter with dynamic shape prior," *IEEE Tran. on Image Processing*, vol. 16, no. 5, pp. 1370 – 1382, 2007.

[5] D. Mukherjee and S. Acton, "Geoscience and remote sensing, ieee transactions on," *IEEE Transactions on Geoscience and Remote Sensing*, vol. 40, no. 2, pp. 405 – 415, 2002.

[6] T. Laet, H. Bruyninckx, and J. Schutter, "Shape-based online multitarget tracking and detection for targets causing multiple measurements: Variational bayesian clustering and lossless data association," *IEEE Transactions on Pattern Analysis and Machine Intelligence (PAMI)*, vol. 33, pp. 2477 – 2491, 2011.

[7] J. Wang and Y. Yagi, "Integrating color and shape-texture features for adaptive real-time object tracking," *IEEE Transactions on Image Processing*, vol. 17, no. 2, pp. 235 – 240, February 2008.

[8] W.-C. Lin and Y. Liu, "A lattice-based mrf model for dynamic near-regular texture tracking," *IEEE Transactions on Pattern Analysis and Machine Intelligence*, vol. 29, no. 5, pp. 777 – 792, May 2007.

[9] O. Harant, L. Bombrun, G. Vasile, L. Ferro-Famil, and M. Gay, "Displacement estimation by maximum-likelihood texture tracking," *IEEE Journal of Selected Topics in Signal Processing*, vol. 5, no. 3, pp. 398 – 407, June 2011.

[10] M. Cascia, S. Sclaroff, and V. Athitsos, "Fast, reliable head tracking under varying illumination: an approach based on registration of texture-mapped 3d models," *IEEE Transactions on Pattern Analysis and Machine Intelligence (PAMI)*, vol. 22, no. 4, pp. 322 – 336, April 2000.

[11] A. Shahrokni, T. Drummond, F. Fleuret, and P. Fua, "Classification-based probabilistic modeling of texture transition for fast line search tracking and delineation," *IEEE Transactions on Pattern Analysis and Machine Intelligence (PAMI)*, vol. 31, no. 3, pp. 570 – 576, March 2009.

[12] S. P. Chowdhury, K. Rafferty, and A. Das, "Localisation and tracking of an airport's approach lighting system," in *Proceedings of the 2010 international conference on Computer vision and graphics, ICCVG 2010*, Warsaw, Poland, 20 - 22 September 2010, pp. 19 – 26.

[13] S. P. Chowdhury, K. Rafferty, and S. Ferguson, "Modelling 3d camera movement for vibration characterisation and multiple object identification with application to lighting assessment," in *Proceedings IEEE International Symposium on Robotic and Sensors Environments, ROSE 2011*, Montreal, Canada, 17 - 18 September 2011, pp. 178 – 183.

[14] P. A. Maragos, R. W. Schafer, and M. A. Butt, *Mathematical morphology and its applications to image and signal processing*. Boston : Kluwer Academic, 1996.

[15] J. Goutsias and D. Schonfeld, "Morphological representation of discrete and binary images," *IEEE Transaction on Signal Processing*, vol. 39, pp. 1369 – 1379, June 1991.

[16] A. Morales and R. Acharya, "Statistical analysis of morphological openings," *IEEE Transaction on Signal Processing*, vol. 41, pp. 3052 – 3056, October 1993.

[17] R. Brockett and P. Maragos, "Evolution equations for continuous-scale morphological filtering," *IEEE Transaction on Signal Processing*, vol. 42, pp. 3377 – 3386, December 1994.

[18] N. Bouaynaya, M. Charif-Chefchaouni, and D. Schonfeld, "Spatially variant morphological restoration and skeleton representation," *IEEE Trans. on Image Processing*, vol. 15, no. 11, pp. 3579 – 3591, 2006.

[19] N. Bouaynaya, M. Charif-Chefchaouni, and D. Schonfeld, "Theoretical foundations of spatially-variant mathematical morphology part i: Binary images," *IEEE Transaction of Analysis and Machine Intelligence PAMI*, vol. 30, no. 5, pp. 823 – 836, May 2008.

[20] N. Bouaynaya and D. Schonfeld, "Theoretical foundations of spatially-variant mathematical morphology part ii: Gray-level images," *IEEE Transaction of Analysis and Machine Intelligence PAMI*, vol. 30, no. 5, pp. 837 – 850, May 2008.

[21] J. Serra, *Image analysis and mathematical morphology*, A. Press, Ed. Academic Press, 1982.

[22] H. Heijmans, *Morphological image operators*, ser. Advances in Electronics and Electron Physics Series. Boston: Academic Press, 1994.

[23] R. Lerallut, E. Decenciere, and F. Meyer, "Image filtering using morphological amoebas," *IVC*, vol. 25, no. 4, pp. 395 – 404, 2006.

[24] P. Dokladal and E. Dokladalova, "Grey-scale morphology with spatially-variant rectangles in linear time," *Springer - Advanced Concepts for Intelligent Vision Systems*, pp. 674 – 685, 2008.

[25] O. Tankyevych, H. Talbot, P. Dokladal, and N. Passat, "Direction-adaptive grey-level morphology. application to 3d vascular brain imaging," in *Proceedings of the 16th IEEE International Conference on Image Processing (ICIP 09)*, 2009, pp. 2261 – 2264.

[26] R. Levillain, T. Geraud, and L. Najman, "Milena: Write generic morphological algorithms once, run on many kinds of images," in *In the proceedings of the 9th International Symposium on Mathematical Morphology (ISMM)*, August 2009, pp. 295 – 306.

[27] P. Maragos, "Lattice image processing: A unification of morphological and fuzzy algebraic systems," *J. Math. Imaging Vis.*, vol. 22, no. 2-3, pp. 333 – 353, May 2005.

[28] R. Hirata, J. Barrera, R. Hashimoto, and D. Dantas, "Microarray gridding by mathematical morphology," in *Proceedings of XIV Brazilian Symposium on Computer Graphics and Image Processing, 2001*, October 2001, pp. 112 – 119.

[29] R. Hirata, J. Barrera, R. Hashimoto, and D. Dantas, "Segmentation of microarray images by mathematical morphology," *Real-Time Imaging*, vol. 8, no. 6, pp. 491 – 505, December 2002.

[30] P. Maragos and C. Vachier, "Overview of adaptive morphology: Trends and perspectives," in *Proceeding of 16th IEEE International Conference on Image Processing, ICIP 2009*, November 2009, pp. 2241 – 2244.

[31] M. Ito, M. Tsubai, and A. Nomura, "Morphological operations by locally variable structuring elements and their applications to region extraction in ultrasound images," *Systems and Computers in Japan*, vol. 34, no. 3, pp. 33 – 43, March 2003.

[32] S. Beucher, J. M. Blosseville, and F. Lenoir, "Traffic spatial measurements using video image processing," in *Proceedings of SPIE's Advances in intelligent robotics systems. Cambridge symposium on optical and optoelectronic engineering*, Cambridge, Mass, USA, 1987.

[33] O. Cuisenaire, "Locally adaptable mathematical morphology using distance transformations," *Pattern Recognition*, vol. 39, no. 3, p. 405 416, 2006.

[34] F. Dias, J. Cousty, and L. Najman, "Some morphological operators on simplicial complex spaces," *Lecture Notes in Computer Science*, vol. 6607, pp. 441 – 452, 2011.

[35] J. Cousty, L. Najman, and J. Serra, "Some morphological operators in graph spaces," in *Proc. of the 9th Int. Symposium on Mathematical Morphology and Its Application to Signal and Image Processing (ISMM 09)*, Groningen, The Netherlands, 2009, pp. 149 – 160.

[36] R. Hirata, J. Barrera, F. Flores, and R. Lotufo, "Automatic design of morphological operators for motion segmentation," in *Proceedings of XII Brazilian Symposium on Computer Graphics and Image Processing, 1999*, 1999, pp. 283 – 292.

[37] R. Hirata, J. Barrera, and R. Terada, "Text segmentation by automatically designed morphological operators," in *Proceedings of XIII Brazilian Symposium on Computer Graphics and Image Processing, 2000*, 2000, pp. 284 – 291.

[38] L. Chockalingam and B. DayaSagar, "Mapping of sub-watersheds from digital elevation model: A morphological approach," *International Journal of Pattern Recognition and Artificial Intelligence (IJPRAI)*, vol. 17, no. 2, pp. 269 – 274, 2003.

[39] A. K. Das and B. Chanda, "Text skew detection: A morphological approach," *Journal of Institute of Engineers (I).*, vol. 78 November, pp. 1–4, 1997.

[40] L. Najman, H. Talbot *et al.*, *Mathematical morphology: from theory to applications*. ISTE-Wiley, 2010.

[41] J. Barrera, E. Dougherty, and M. Brun, "Hybrid human-machine binary morphological operator design. an independent constraint approach," *Signal Processing*, vol. 80, pp. 1469 – 1487, 2000.

[42] P. Maragos and C. Vachier, "A pde formulation for viscous morphological operators with extensions to intensity-adaptive operators," in *Proceeding of 15th IEEE International Conference on Image Processing, ICIP 2008*, October 2008, pp. 2200 – 2203.

[43] S. Lim, B. DayaSagar, V. Koo, and L. Tay, "Morphological convexity measures for terrestrial basins derived from digital elevation models," *Computers & Geosciences*, vol. 37, pp. 1285 – 1294, 2011.

[44] J. Niblock, J. Peng, K. McMenemy, and G. Irwin, "Fast model-based feature matching technique applied to airport lighting," *IET Science, Measurement and Technology*, vol. 2, no. 3, pp. 160 – 176, 2008.

[45] C. Tomasi and T. Kanade, "Detection and tracking of point feature," Shape and Motion from Image Streams: a Factorization Method-Part 3,, Tech. Rep. CMU-CS-91-132, April 1991.

[46] J. Shi and C. Tomasi, "Good features to track," in *Proceedings of the IEEE Computer Society Conference on Computer Vision and Pattern Recognition CVPR'94*, 1994, pp. 593 – 600.

[47] D. Lowe, "Object recognition from local scale-invariant features," in *International Conference on Computer Vision, ICCV'99*, Corfu, Greece, 1999, pp. 1150 – 1157.

[48] D. Lowe, "Local feature view clustering for 3d object recognition," in *IEEE Conference on Computer Vision and Pattern Recognition CVPR'01*, Hawaii, 2001, pp. 682 – 688.

[49] S. P. Chowdhury, K. Rafferty, and S. Ferguson, "Confidence factor determination for performance evaluation of lighting pattern," in *Proceedings 13th Int. IEEE Conference on Intelligent Transportation Systems, ITSC 2010*, Madeira, Portugal, 19 - 22 September 2010, pp. 1380 – 1387.

[50] J. Serra, *Image Analysis and Mathematical Morphology*. London: Academic Press, 1982.

[51] ICAO. International Civil Aviation Organization, *Aerodrome design and operations, annex 14, vol.1, 4th Edition*, Std., July 2004.

[52] J. Hopcroft and J. Ullman, *Introduction to automata theory, languages, and computation*. Addison-Wesley, 1979.

[53] R. Gonzalez and R. Woods, *Digital Image Processing*. Prentice Hall, 2007, no. ISBN: 978-0-13-168728-8.

[54] T. Zhang and C. Suen, "A fast parallel algorithm for thinning digital patterns," *Communications ACM*, vol. 27, no. 3, pp. 236 – 239, 1984.

[55] S. P. Chowdhury, K. Rafferty, and S. Ferguson, "Simulation and performance assessment of airport landing lighting," in *Proceedings 13th Int. IEEE Conference on Intelligent Transportation Systems, ITSC 2010*, Madeira, Portugal, 19 - 22 September 2010, pp. 1600 – 1607.

Shyama Prosad Chowdhury (M'07) received a BE (Honours) in Computer Science and Engineering from Vidyasagar University, India (2002), a ME in Computer Science and Technology from Bengal Engineering and Science University, Shibpur, India (2004) followed by a PhD in the field of image processing and computer vision (2012) from the School of Electrical and Electronic Engineering, Queen's University Belfast, UK.

He has over seven years of prolific research experience in R&D division of Avisere Technology PL and Videonetics Technology PL. His research interests include mobile camera technology, video surveillance, content basted image retrieval, medical image analysis, document image processing, mathematical image morphology and computer vision.

Karen Rafferty has over ten years experience working within the fields of image processing, computer vision, and intelligent devices that can perceive their environment and respond to it. Dr Rafferty has authored over 30 journal and conference papers in the area of intelligent devices, computer vision, image processing and applications of virtual reality. Her first book on Virtual Reality was published in 2007.

Stuart Ferguson has over 25 years experience in computer graphics and software engineering. He is the author of the book "Practical Algorithms for 3D computer Graphics" (2001) He is currently a lecturer in the School of Electronics, Electrical Engineering and Computer Science at the Queen's University of Belfast where he is researching on real-time application program implementations for mobile devices.